Durham E-Theses

Liquid repellent surfaces

Coulson, Stephen Richard

How to cite:

Coulson, Stephen Richard (2000) *Liquid repellent surfaces*, Durham theses, Durham University. Available at Durham E-Theses Online: http://etheses.dur.ac.uk/761/

Use policy

Liquid Repellent Surfaces

Ph.D. Thesis

by

Stephen Richard Coulson

Department of Chemistry

University of Durham

1999

For Mum and Dad

STATEMENT OF COPYRIGHT

DECLARATION

The work described in this thesis was carried out in the Chemistry Department at the University of Durham between October 1996 and September 1999. It is the original work of the author, except where otherwise acknowledged, and has not been submitted previously for a degree at this or any other University.

Solution phase polymerised compounds (Chapter 2) were prepared by Dr. Stuart Brewer (DERA) and Atomic Force Microscopy work (Chapters 2, 3 and 4) were carried out by Iain Woodward (University of Durham).

PUBLICATIONS

Work carried out in this thesis has been published or will be submitted for publication as follows:-

(1)   S. R. Coulson, J. P. S. Badyal, C. Willis, S. Brewer, Eur. Pat. 9712338.4 (filed June 1997).

(2)   S. R. Coulson, J. P. S. Badyal, C. Willis, S. Brewer, Eur. Pat. 9720078.6 (filed September 1997).

(3)   S. R. Coulson, J. P. S. Badyal, C. Willis, S. Brewer, Eur. Pat. 9812457.1 (filed June 1998).

(4)   S. R. Coulson, J. P. S. Badyal, C. Willis, S. Brewer, Eur. Pat. 9816077.3 (filed July 1998).

(5)   S. R. Coulson, J. P. S. Badyal, C. Willis, S. Brewer, The Sunday Times, 11th October 1998, page 3.

(6)   S. R. Coulson, J. P. S. Badyal, C. Willis, S. Brewer, The Independent, 26th October 1998, page 7.

(7)   S. R. Coulson, J. P. S. Badyal, C. Willis, S. Brewer, Eur. Pat. 9827309.7 (filed December 1998).

(8)   S. R. Coulson, J. P. S. Badyal, C. Willis, S. Brewer, Eur. Pat. 9827311.3 (filed December 1998).

(9)   S. R. Coulson, J. P. S. Badyal, C. Willis, S. Brewer, Eur. Pat. 9827312.1 (filed December 1998)

(10)   S. R. Coulson, J. P. S. Badyal, C. Willis, S. Brewer, Eur. Pat. 9827315.4 (filed December 1998).

(11)   S. R. Coulson, J. P. S. Badyal, C. Willis, S. Brewer, Eur. Pat. 9827316.2 (filed December 1998).

(12)   S. R. Coulson, J. P. S. Badyal, C. Willis, S. Brewer, Eur. Pat. 9827318.8 (filed December 1998).

(13)   S. R. Coulson, J. P. S. Badyal, C. Willis, S. Brewer, *Ultra Low Surface Energy Plasma Polymer Films*, Chemistry of Materials, in press.

(14)   S. R. Coulson, J. P. S. Badyal, C. Willis, S. Brewer, *Plasmachemical Functionalisation of Solid Surfaces with Low Surface Energy Perfluorocarbon Chains*, Langmuir, in press.

(15)   S. R. Coulson, J. P. S. Badyal, C. Willis, S. Brewer, *Super-Repellent Fluoropolymer Surfaces*, in preparation.

ACKNOWLEDGEMENTS

ABSTRACT

The work in this thesis is primarily aimed at supporting the NBC (Nuclear, Biological and Chemical) aspect of Crusader 21, the military clothing programme for the early 21st Century. This aims to produce a multi-purpose, systems-orientated combat ensemble for the UK Armed Services. Conventional "wet" techniques for chemically modifying fabrics have certain disadvantages, however employing plasma technology may provide a route for many novel "multi-functional effects" fabrics such as repellency against toxic chemical agents.

In order to produce repellent coatings the surface must have a low surface energy. To obtain this, inert chemical groups need to be attached to the solid substrate. In addition to chemistry, surface roughness plays an important role in repellency.

Liquid repellent surfaces have been produced by the pulsed plasma polymerisation of 1H,1H,2H,2H-heptadecafluorodecyl acrylate. These films have chemical functionalities indicative of polymerisation occurring through the acrylate double bond, as shown by Infrared Spectroscopy analysis. Structural retention was optimised using experimental design techniques and resulted in a critical surface tension of wetting as low as 4.3 mN m^{-1} (c.f. Teflon 18.5 mN m^{-1}). Plasma deposition of a functionalised surface followed by reaction with a fluorinated alcohol proved less affective.

Enhanced deposition rates for 1H,1H,2H-perfluorododec-1-ene, over the saturated analogue, have indicated that polymerisation can occur during the off-time of the pulsed plasma period, via free radical polymerisation pathways. X-ray Photoelectron Spectroscopy (XPS) has indicated greater structural group retention for monomers containing double bonds.

In order to obtain super liquid repellency the effect of surface roughness was investigated, where both commercially available rough surfaces and plasma roughened substrates were utilised. Once optimised, the rough surfaces were coated with 1H,1H,2H,2H-heptadecafluorodecyl acrylate and produced super repellent films.

CONTENTS

CHAPTER 1

AN INTRODUCTION TO PLASMAS, REPELLENT SURFACES AND EXPERIMENTAL TECHNIQUES

CHAPTER 2

ULTRA LOW SURFACE ENERGY PLASMA POLYMER FILMS

CHAPTER 3

PLASMACHEMICAL FUNCTIONALISATION OF SOLID SURFACES WITH L SURFACE ENERGY PERFLUOROCARBON CHAINS

CHAPTER 4

ROUGH SURFACES

CHAPTER 5

FLUOROCARBON LABELLING OF A FUNCTIONALISED PLASMA POLYMER LAYER — 102

CHAPTER 6

CONCLUSIONS — 120

APPENDIX — 122

CHAPTER 1

AN INTRODUCTION TO PLASMAS, REPELLENT SURFACES AND EXPERIMENTAL TECHNIQUES

1.1. INTRODUCTION

To date, many methods for the production of repellent coatings have been carried out in the solution phase and have hence been limited to a narrow group of substrates with specific functional groups [1]. The unfavourable energetics of these processes make them inapplicable to an extremely wide number of possible everyday applications including biocompatibility, sports and outdoor clothing, lithography and aerospace [2]. Carrying out reactions in the gas phase is more desirable as the reactive species have greater mobility and a greater chance of reacting. Plasma chemistry is the production of an ionised gas and over the last 30 years has become popular, for surface modification and the deposition of polymer films. It is the aim of this chapter to introduce the concepts of plasma chemistry, repellency, and to describe the analytical techniques used throughout this thesis.

1.2. PLASMAS

1.2.1. Introduction

A plasma (or electrical discharge [3]) is a partially or fully ionised gas and is often referred to as the fourth state of matter. The term was first used by Langmuir in 1929 [4] to describe the state which makes up the vast majority of the known universe, mainly in the form of stars. A plasma consists of many reactive media including electrons, positive and negative ions, neutrals, metastables and electromagnetic radiation [5], [6], all of which are capable of participating in or initiating reactions [7]. In order to be termed a plasma there must be an equal number of positive and negative species present, although local perturbations from neutrality occur, the overall charge must be neutral.

1.2.2. Equilibrium and Non-Equilibrium Plasmas

Plasmas can be categorised into three types, depending on the method of ionisation and the physical properties they possess. Complete thermodynamic equilibrium plasmas exist when all constituent species are at the same temperature, such a state occurs in stars. Plasma jets and electric arcs are examples of local thermodynamic plasmas where the temperature of all the species except the radiation are equal. These two processes lead to very dense plasmas at extremely high temperatures, termed "hot" plasmas, and can be used to initiate many thermal reactions, such as in metallurgy [6]. The third type is a non-equilibrium plasma where the electron temperature, typically ~ 10,000 K, far exceeds that of the bulk gas, ~300 - 500 K. This is termed a glow discharge and is used to carry out non-thermally activated reactions, which is the type of plasma used for the work reported in the following chapters. Glow discharges are produced by passing an electrical field around or through a low pressure gas or vapour. Under normal conditions the degree of ionisation is relatively low and there are many neutrals present at ambient temperatures [7], [8]. Processes occurring include plasma polymerisation [9] and etching mechanisms [10], both resulting from low temperature non-equilibrium plasmas.

1.2.3. Plasma Ignition

In the processes that will be discussed in the following chapters a glow discharge is achieved by passing a radio frequency (R.F.) oscillating electric field around a low pressure gas or vapour. In order to ignite the plasma, energy supplied to the system must be greater than the ionisation energy of the gas molecules. The applied energy has the effect of accelerating randomly occurring free electrons [11] which can undergo elastic and inelastic collisions, the latter leading to ionisation and the production of secondary electrons [6]. Once ignition has occurred a lower power can be used in order to sustain the plasma glow, as the initial ionisation produces many reactive components which can go on to cause more excitation and ionisation via a cascade effect.

For plasma stability it is a requirement that the quasi-neutral nature of the system is maintained. This can only be achieved if the discharge volume is greater than the Debye length, λ_D, the distance over which a small potential can perturb a plasma [7], Equation 1.1:

$$\lambda_D = \left(\frac{\varepsilon_o K T_e}{n_e e^2} \right)^{1/2} \qquad 1.1$$

where ε_o is the permittivity of free space, K is Boltzman's constant, T_e is the electron temperature, n_e is the electron density per cm^3 in the plasma phase and e is the charge of an electron. For the non-equilibrium "cold" plasmas studied here, T_e and n_e are typically 1 eV and 10^{10} respectively, giving a Debye length of 74 μm. Local charge concentrations within the plasma phase are confined to λ_D. Minimisation of any electrical fields created in the plasma are achieved by the redistribution of charged particles, where the electrons respond much quicker than the heavier ions to reduce the field. This results in Debye shielding, which gives rise to the quasi-neutrality of the plasma. A consequence of this is the production of a plasma potential due to the initial rapid acceleration of the electrons to the reactor walls, leaving a net positive charge in the plasma. The result is a potential difference between the reactor walls and the plasma bulk [7], [8].

1.2.4. Electron Energy

Ionisation reactions occurring in the glow discharge are essential to sustain the plasma [7]. As these are caused by electrons, it is important to know their energy distributions which describe the range of energies possessed by a certain average electron energy. The first distribution function assumes that $T_e = T_g$, that is the temperature of the electrons equals that of the gas, which takes the form of a Maxwellian distribution [7]. This is more appropriate for thermal plasmas. The Druyvesteyn distribution [7] is more fitting for non-equilibrium plasmas as it takes into account the electron temperature being much greater then that of the ions, $T_e \gg T_i$, Equation 1.2 and Figure 1.1.

$$f(W) = 1.04 W_{av}^{-3/2} W^{1/2} \exp\left(-\frac{0.55 W^2}{W_{av}^2} \right)$$

1.1

Where W_{av} is the average energy of electrons. What is evident from the 4 curves is that they all have a high energy tail, somewhat greater than the average electron energy. These high energy electrons play an important role in the chemistry and physical conditions of the plasma.

1.2.5. Mechanisms Occurring During Plasma Polymerisation

The basic polymerisation steps of initiation, propagation and termination that occur during solution phase techniques are also present in glow discharges, but are inherently more complicated [7]. Re-initiation can also occur, both in the gaseous plasma or on the surface of the substrate / reactor walls. Figure 1.2 illustrates the depths to which various reactive species in the plasma can penetrate. The vacuum-ultraviolet (VUV) radiation can penetrate the deepest [12], 1-10 μm and has sufficient energy to break chemical bonds. Electrons penetrate depths of between 5–75 Å due to their relative high energies and ions and neutrals between 1-10 Å. There are a large number of reactive species present in the plasma phase, leading to a number of reactions. When

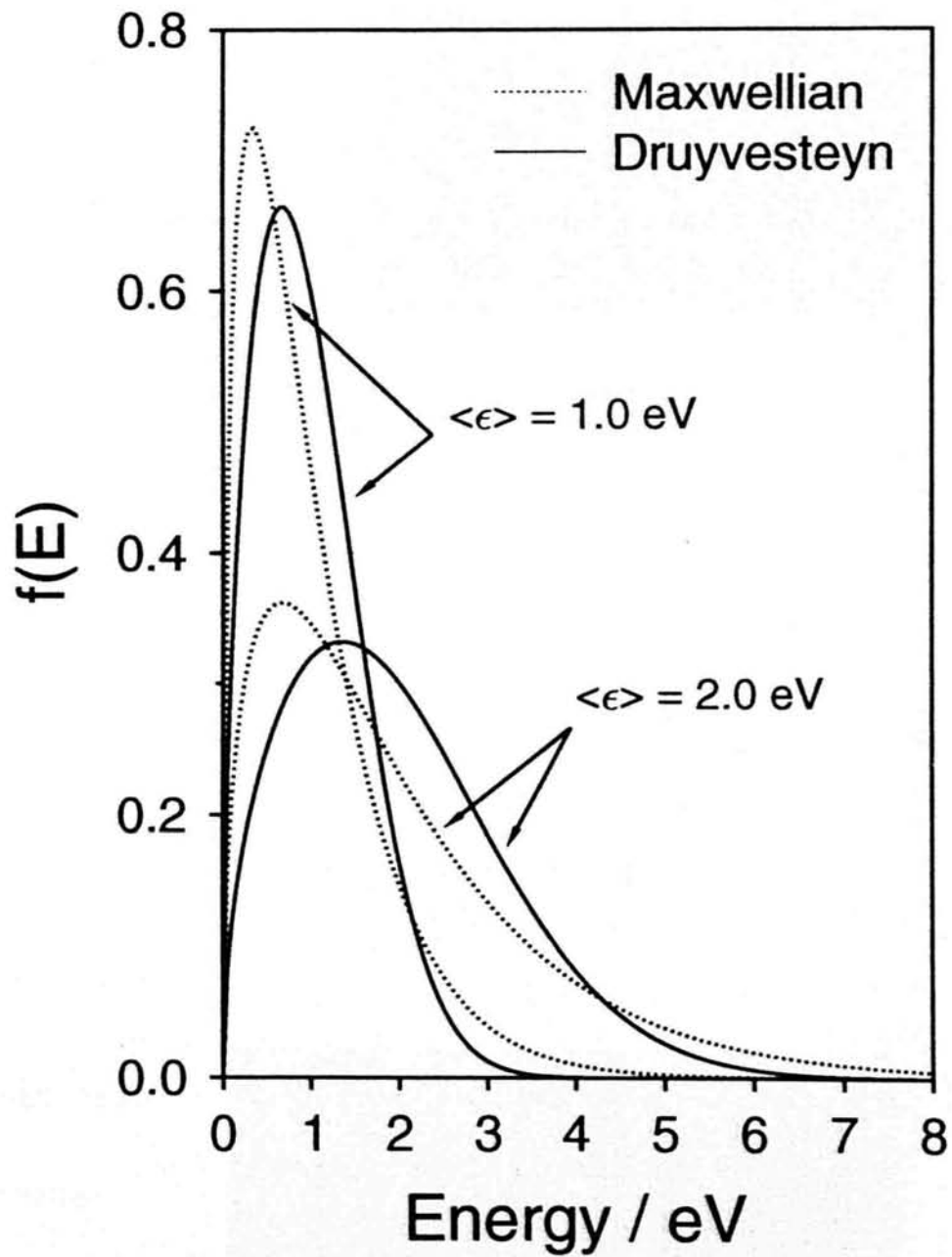**Figure 1.1** Maxwellian and Druyvestyn plasma electron energy distributions for average electron energies of 1 and 2 eV [7].
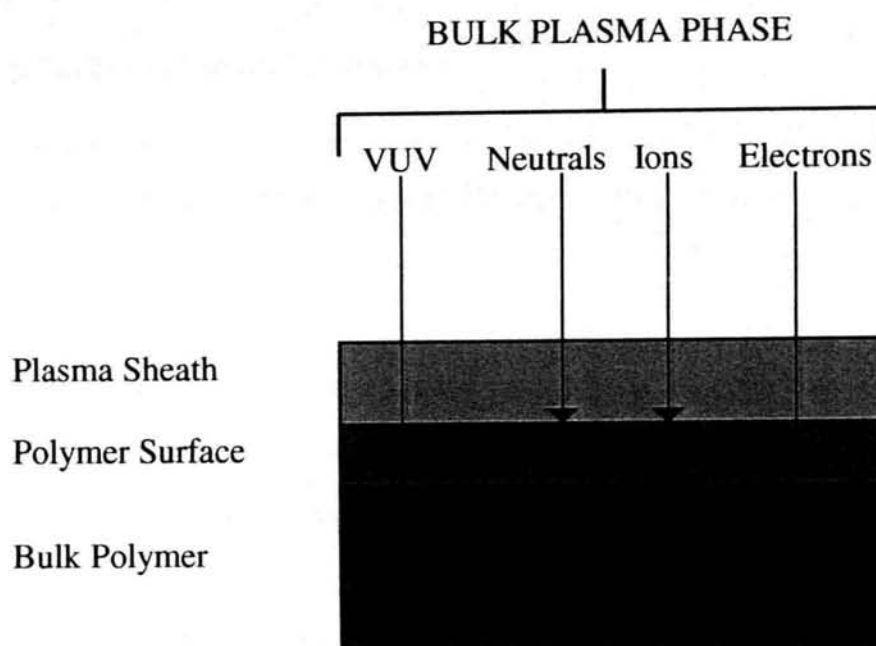
Figure 1.2 Depths of penetration of species in the plasma phase [12].
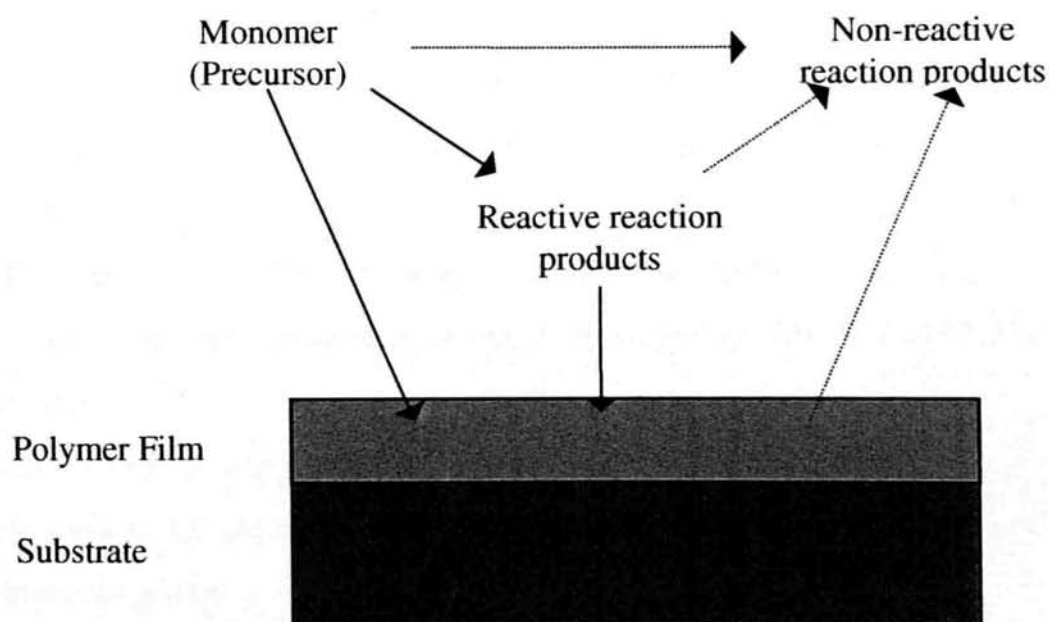
Figure 1.3 Schematic of the numerous reaction pathways that can occur during plasma polymerisation [13]. The solid lines indicate deposition and the broken lines the volatile product formation pathways.

1.2.6. Advantages of Plasma Processes

Regardless of the inherent complexity of plasma processes, there are numerous advantages [14] over conventional methods which have fuelled the growth of this industry over recent years:-

- Reactions are carried out in an enclosed glass chamber where any waste or by-products can be frozen out for safety and ease of disposal.
- Very small amounts of precursor are needed so the cost and environmental impact are low.
- Treated substrates can easily be re-coated which makes many products reusable.
- Plasma polymer film thickness can be easily controlled, from a few angstroms to the micron level.
- Polymer films or functional group modifications tend to be well adhered and form strong bonds with a variety of substrates including, polymers, metals, ceramics, fabrics and glass.
- Plasma polymer films are pin-hole free.
- Multilayer films can be produced with varying chemical or physical properties.
- Gas, liquid and solid monomers can be used as precursor materials for a variety of reactions.
- All morphologies can be coated, as the deposition medium is a gas.
- By using different conditions, a range of properties may be tailored to the solid surface.
- Bulk properties are unaffected by the surface process, giving rise to numerous applications for materials with desirable bulk properties but inappropriate surface functional groups.

1.2.7. Reactor Set-Up and Matching

The reactor set-up consists of an enclosed glass reactor, pumped to low pressure (typically 3×10^{-2} mbar) via a liquid nitrogen cold trap, Figure 1.4.

A gas or vapour is allowed into the main reaction chamber until a constant pressure is attained. An R.F. signal, at a frequency of 13.56 MHz, can then be applied to the

system, leading to gas breakdown and the formation of a glow discharge. These radio frequency discharges are classed as electrodeless discharges as the electrodes are not in contact with the plasma phase. This method of ionisation has the added advantage of avoiding contamination of the products via electrode decomposition or sputtering. The power being supplied to the plasma passes through an externally wound copper coil and
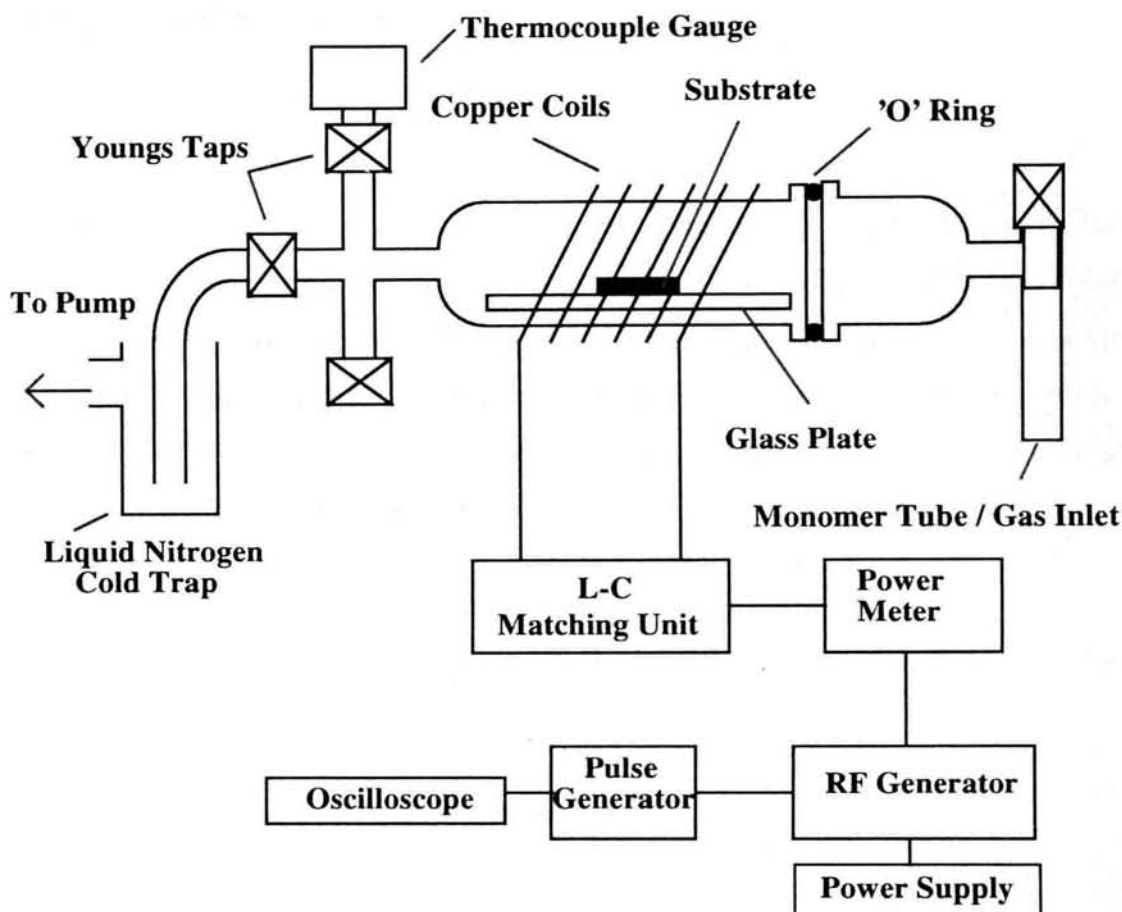
Figure 1.4 Typical reactor design for the production of low temperature plasmas.

is controlled by the R.F. generator. The matching unit is used to couple the output impedance of the R.F. generator [7] with that of the partially ionised gas; this is achieved by minimising the standing wave ratio.

1.2.8. Continuous Wave Plasmas

On production of the plasma, the glow discharge will remain as long as the system is sustained by the R.F. generator, providing it remains matched. This is known as a continuous wave, CW, plasma as a constant power is supplied throughout. Plasmas formed by CW techniques often use high powers, 10 - 100 W, which are very effective

8

for producing complete gas breakdown and high energy reactive species. This can lead to numerous surface modification processes of both a physical and chemical nature, such as functional group modification [15], etching [16], and polymerisation [17]. Whilst novel coatings produced from this random deposition have made a large commercial impact, precursor functional group retention and control of plasma phase chemistry has long been sought after.

1.2.9. Pulsed Plasmas

By connection of a pulse generator and an oscilloscope to the R.F. generator (Figure 1.4), the peak power being supplied to the system can be modulated leading to lower average powers. This is achieved by setting up a pulse on (t_{on}) and off-time (t_{off}) using the pulse generator, which can be monitored on the oscilloscope. The duty cycle is defined as $t_{on}/(t_{on}+t_{off})$. The peak power supplied, P_P, can also be varied on the R.F. generator resulting in an average power output ($<P>$) as shown by Equation 1.3:

$$< P >= P_P \left(\frac{t_{on}}{t_{on} + t_{off}} \right)$$

1.3

This can be displayed schematically, Figure 1.5:

Figure 1.5 Schematic drawing indicating how the pulsing parameters are assigned.

Pulsing the plasma not only leads to lower average powers, but could allow polymerisation to occur during the plasma off-time, without obliteration of the parent structure. This results in polymer films with functional properties resembling that of
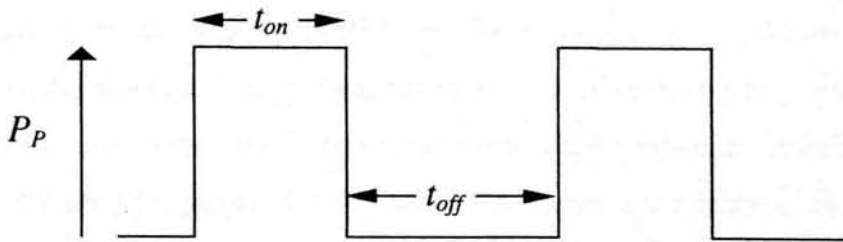
the starting material. To achieve this it is necessary to tune the pulsing parameters, t_{on}, t_{off} and P_P.

1.3. SURFACES

1.3.1. Introduction

Surfaces differ both chemically and physically from the bulk phase [18], [19], [20], as they are in contact with a different environment. Most noticeably, the orientation and packing [21] of polymer chains differ between the two phases due to the different intermolecular forces to which each one is exposed. Surface properties are dependent on the environment, as a system will tend to minimise the interfacial energy by matching the surface energy with that of the environment. This can be achieved by re-orientation of surface functional groups or migration of certain moieties from, or into, the bulk phase. Interactions between solid surfaces and liquids generally arise from the residual electronic field of the valence electrons present in both media and leads to processes such as adhesion and wetting. This is supported by Langmuir's principal of independent surface action which states that interactions at surfaces are primarily due to the uncompensated fields emanating from the outermost molecular layers [22]. There are three types of intermolecular attractions which can cause adhesion or wetting of a surface by a liquid: dispersive forces; orientation forces; and inductive forces. Dispersive forces are common to all molecules and are caused by interactions between the fluctuating electron clouds of molecules present in both phases. Orientation forces occur between molecules which have permanent dipole-moments where the molecules rotate to attract each other. Thirdly, inductive forces arise when a dipole-moment in one phase can induce a temporary dipole-moment in the other phase, thus giving rise to attraction. The interfacial energy arises from the sum of these intermolecular forces and represents the total work which must be done on the system to form the interface.

1.3.2. Repellent Coatings

In order for a surface to show repellent properties it is necessary that it possesses low surface energy, where surface energy is the sum of the interaction energies present at a surface.

The word repellency is a universally used term to describe commercially available, "non-stick" coatings such as Teflon™ and Gore-Tex™. Technically, it is incorrect to describe such coatings as repellent as they do not "repel" liquids but simply do not interact with them (or have limited interactions). A more correct term to use would be inert, but as it is extremely unlikely that such a popular concept will ever be changed, repellency will be used throughout this thesis.

There are two important factors that play a role in repellency, surface chemistry and surface roughness (the latter will be discussed in Chapter 4). Previously, common ways to produce repellent or hydrophobic (water repellent) coatings was the use of either hydrocarbon or silicone finishes. However, if oil repellency (oleophobicity) is required, fluorochemical coatings are necessary due to their much lower surface energy values [23]. The reason for this lies with the fundamental properties of the fluorine atom, whose low polarisability and high ionisation energy results in very weak inter- and intramolecular interactions within fluorocarbons [24]. Fluorine's relatively small size and tightly bound non-bonding electrons make interactions difficult. Also the high electronegativity of fluorine, coupled with its' high degree of 2s and 2p orbital overlap with the corresponding orbitals on the carbon atom, help to explain why saturated fluorocarbons are the lowest known surface tension liquids at room temperature [24]. The degree of repellency resulting from such coatings will depend on both the molecular structure of the fluorocarbon and non-fluorinated segment of the compound, as well as the surface topography [23].

1.3.3. Theory

There is an 'excess energy in the surface' of a solid or a liquid. This can be understood by considering the energy needed to form a surface, by breaking the bonds across what are to become the two surfaces formed, Figure 1.6.
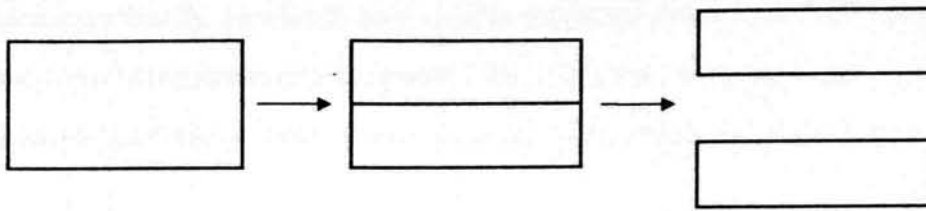
Figure 1.6 Excess energy present at a surface [25].

Liquids are commonly referred to as having surface tensions, a force that acts in a direction parallel to the boundary surface of a liquid and tends to minimise surface area. That is a geometrical shape with the smallest surface area to volume ratio, i.e. a sphere. The reason that this is the preferred shape is because molecules in the body of a liquid are equally attracted in all directions by the other molecules present but those at the surface tend to have a net residual inward pull. In order to increase the surface area, work has to be done against the surface tension. Surface energy is defined as the work necessary to increase the surface by unit area against the force of surface tension and is the term used for solid surfaces. Surface energy and surface tension are denoted by the symbol γ and the subscripts incorporated describe the interface concerned.

When a polymer surface is wetted by a liquid, the energy available to bring about the wetting process is the difference between the surface energy of the solid / vapour and solid / liquid interface, γ_{SV} and γ_{SL} respectively, Figure 1.7.
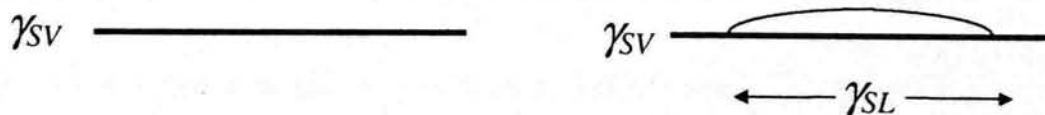
Figure 1.7 Wetting of a solid surface [20].

The process occurring in Figure 1.7 can be related to the adhesion tension, τ, Equation 1.4.

$$\tau = \gamma_{SV} - \gamma_{SL}$$
1.4

This has very little practical use as there is no method of measuring the surface energy components directly, as elastic and viscous restraints within the bulk phase prevent a surface from being reversibly deformed [26]. This has led to attempts to evaluate τ by considering the contact angle, θ, formed at the three phase boundary, Figure 1.8.
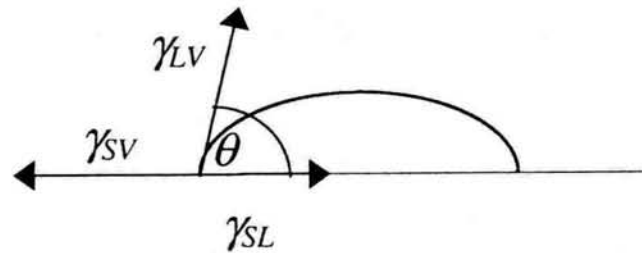
Figure 1.8 Contact angle formed at the three phase boundary.

In order to calculate the surface energy it is first necessary to relate the surface energy components to θ. This can be done by considering the wetting phenomenon illustrated below, Figure 1.9.
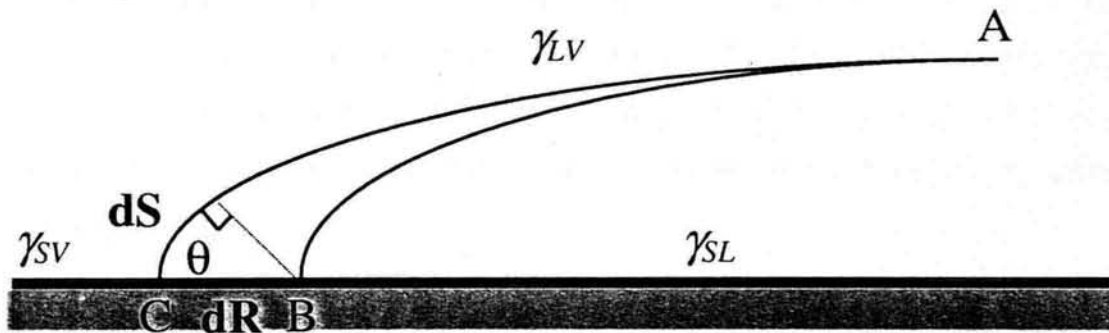
Figure 1.9 Schematic of the spreading of a liquid droplet on a solid surface [27].

Here we say that a droplet of liquid on a surface forms a periphery **A-B** (here we consider just half the droplet). This droplet then spreads until the equilibrium position is reached i.e. the droplet now resides at **A-C**. The change in Gibbs' free energy at constant volume can be related to the change in area, Equations 1.5 to 1.10:

$$dG = 2\pi RdR\gamma_{SV} - 2\pi RdR\gamma_{SL} - 2\pi RdS\gamma_{LV} \qquad 1.5$$

and from trigonometry

$$dS = dR\cos\theta \qquad 1.6$$

so

$$dG = 2\pi R dR \gamma_{SV} - 2\pi R dR \gamma_{SL} - 2\pi R dR \cos\theta \gamma_{LV} \qquad 1.7$$

which simplifies to

$$dG = 2\pi R dR (\gamma_{SV} - \gamma_{SL} - \gamma_{LV}\cos\theta) \qquad 1.8$$

At equilibrium contact angle $dG = O$ therefore:

$$0 = \gamma_{SV} - \gamma_{SL} - \gamma_{LV}\cos\theta \qquad 1.9$$

so

$$\gamma_{SV} = \gamma_{SL} + \gamma_{LV}\cos\theta \qquad 1.10$$

Equation 1.10 is more commonly known as Young's equation [28] and relates the contact angle to the individual surface energy components. However it neglects a force term normal to the surface, which arises due to viscous and elastic restraints in the bulk phase.

Surface energy of a material is the excess energy per unit area or force per unit length and adopts the units mJ m^{-2} or mN m^{-1} respectively. There are several formulations of Equation 1.10 which have resulted from different interpretations of the relationship between contact angle and molecular interactions present between the surface and the liquid in contact.

Modern contact angle theory has made it possible to calculate surface energy using the contact angles of different liquids having known polar and dispersive surface energy components. Theories include: geometric-mean method; harmonic-mean method and the acid-base theory.

1. Geometric-Mean Theory

This was first used by Fowkes [29] who tried to ascertain the role which dispersive forces play in determining contact angles of various liquids on non-polar (hydrophobic) surfaces. He deduced that there would be a surface energy averaging between a solid and a liquid if they were to come into contact, and assumed the geometric-mean based on an analogy with intermolecular forces in solution. Hence, if $\gamma_{a(ab)}$ is the surface energy of phase a at the interface with phase b then:

$$\gamma_{a(ab)} = \gamma_a - (\gamma_a \gamma_b)^{1/2}$$ 1.11

and similarly,

$$\gamma_{b(ab)} = \gamma_b - (\gamma_a \gamma_b)^{1/2}$$ 1.12

These two equations, taking into account the interfacial energy (γ_{ab}) must be the sum of the free energies of each of the surfaces forming the interface, and has led to Equation 1.13 [30], [31], [32]:

$$\gamma_{ab} = \gamma_a + \gamma_b - 2(\gamma_a \gamma_b)^{1/2}$$ 1.13

Fowkes assumed that the total surface energy was the sum of the dispersive and polar components [33], Equation 1.14.

$$\gamma_s = \gamma_s^d + \gamma_s^p$$ 1.14

Combining the geometric-mean equation with Young's equation gives Equation 1.15, the geometric-mean equation:

$$\left(1 + \cos\theta_i\right)\gamma_i = 2\left[\left(\gamma_i^d \gamma_s^d\right)^{1/2} + \left(\gamma_i^p \gamma_s^p\right)^{1/2}\right]$$ 1.15

Since the dispersive, polar and total surface tensions, γ_i^d, γ_i^p and γ_i respectively, of the liquid are known, along with the measured contact angle, θ_i, the surface energy can be calculated. This is achieved by solving simultaneous equations formed for a least two liquids, one of which must be polar. This will result in the dispersive and polar components of the surface, γ_s^d and γ_s^p respectively, which can be summed for the total surface energy value.

2. Harmonic-Mean Method

This method uses the contact angles of a minimum of two known surface tension liquids, both of which must be polar, and uses the harmonic-mean equation as the method of averaging, Equation 1.16:

Also known as the reciprocal mean equation based on force additivity, this equation has been proposed by Wu [34] for the use of polar liquids interacting on polar (hydrophilic) surfaces.

3. Acid-Base Theory

A recent surface energy theory suggested by Good and van Oss [35] uses three parameters, dispersive (γ_i^d), acid (γ_i^+) and base (γ_i^-) to better describe the surface free energy. This is because there are two types of hydrophilic behaviour [25], Lewis basicity, γ^-, (electron-donating or proton accepting), and Lewis acidity, γ^+, (electron accepting or proton donating). The total surface tension of a liquid is the sum of its dispersive (apolar) and polar components: $\gamma_i = \gamma_i^d + 2(\gamma_i^+ \gamma_i^-)^{1/2}$. Combining the geometric-mean equation with Youngs's equation gives, Equation 1.17:

$$\left(1 + \cos\theta_i\right)\gamma_i = 2\left[\left(\gamma_i^d \gamma_s^d\right)^{1/2} + \left(\gamma_i^+ \gamma_s^+\right)^{1/2} + \left(\gamma_i^- \gamma_s^-\right)^{1/2}\right] \qquad 1.17$$

To solve for γ_s^d, γ_i^+ and γ_i^-, contact angles must be obtained with a minimum of three different, completely characterised liquids, two of which must be polar.

1.3.4. Contact Angle Hysteresis

Contact angle hysteresis is the difference between advancing and receding contact angles and was observed by Rayleigh in 1890 [36]. This arises because in real systems a liquid drop on a solid surface can have many different stable angles due to many closely spaced metastable states. These vary between the advancing (when the plate is wetted for the first time) and receding (when the plate is dragged back out of the wetting liquid). Contact angle hysteresis is a useful probe of the real nature of solid surfaces.

There are two main types of contact angle hysteresis. Kinetic hysteresis, which may arises as many commonly used liquids do not behave as neutral probes. This leads to

time dependant surface modifications, arising from processes such as swelling, penetration, surface mobility and surface group re-orientation [37]. Secondly, thermodynamic contact angle hysteresis arises from surface roughness or surface heterogeneity [37].

1.4. CHARACTERISATION TECHNIQUES

1.4.1. X-ray Photoelectron Spectroscopy (XPS)

XPS is a very surface sensitive technique, probing between 1 - 5 nm [38] of the sample surface [39]. It requires ultra-high vacuum as soft X-rays are focused on a sample surface. The radiation leads to the photo-ejection [40] of core level electrons which pass through an electron analyser prior to detection. This results in a spectrum of electron intensity as a function of kinetic energy (KE). The binding energy (BE) of the electrons can be calculated from Equation 1.18:

$$KE = h\nu - BE - \phi \qquad\qquad 1.18$$

where $h\nu$ is the exciting X-ray energy and ϕ is the spectrometer work function. The two most common elements used for X-ray sources are magnesium and aluminium. The reasons for their popularity are: the line width must not limit the energy resolution required in the technique; and the characteristic energy must be high enough to photo-eject a wide range of core level electrons for thorough analysis. Mg Kα (energy of 1253.6 eV and a line width of 0.7 eV) and Al Kα (energy of 1486.6 eV with a line width of 0.85 eV) meet both these requirements.

All atoms present at the sample surface, except hydrogen and helium, are detectable by XPS as they posses both valence and core level electrons. The binding energy of the latter are characteristic of an individual atom and its' environment. For example, all photo-ejected electrons of a particular atom will have a certain binding energy which will only vary by several eV due to different chemical environments that the atom could be in (e.g. oxygenated, fluorinated). Once the analysis has been made, the resulting spectrum is often displayed as BE plotted against intensity and will usually be in the form of an envelope, which displays all the chemical environments. Once these have

17

been obtained for all elements in the sample, the chemical abundances and functional groups present at the surface will be evident. The reason for the surface sensitivity of this technique lies with the small inelastic mean free path of electrons in a solid and depends on the electron energy and the material it is moving through. The electron energies of interest for XPS are from 30 eV to around 2 keV and corresponds to inelastic mean free paths from about 1-5 nm [41], Figure 1.10.
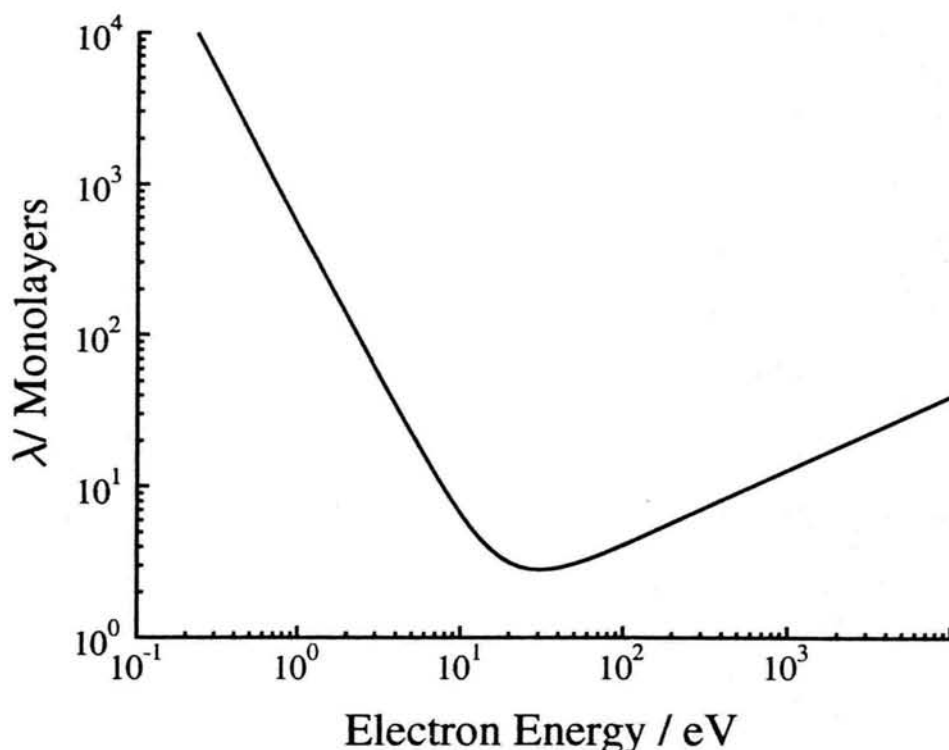
Figure 1.10 Inelastic mean free path of electrons in a solid as a function of energy [41].

The energies of interest for the XPS of polymers are roughly between 100 - 1000 eV and correspond to electrons from only a few monolayers in depth [41]; proving the high surface sensitivity of the process.

Figure 1.11 shows a schematic drawing of an XPS spectrometer. When the filament in the X-ray source becomes incandescent, electrons are produced which accelerate to the face of the anode. X-rays will be produced if the bombarding electrons are of sufficient energy. The photons produced will then pass out of the X-ray source, via an aluminium window and onto the sample.

The photoelectrons pass into the lens system which retards their kinetic energies and focuses them into the concentric hemispherical analyser (CHA). The analyser consists of two concentric hemispheres at potentials $-V_1$ and $-V_2$, where $V_2 > V_1$. By changing the voltage between the plates, electrons of specific kinetic energies will pass through the analyser and into the electron multiplier. The signal is amplified and counts are
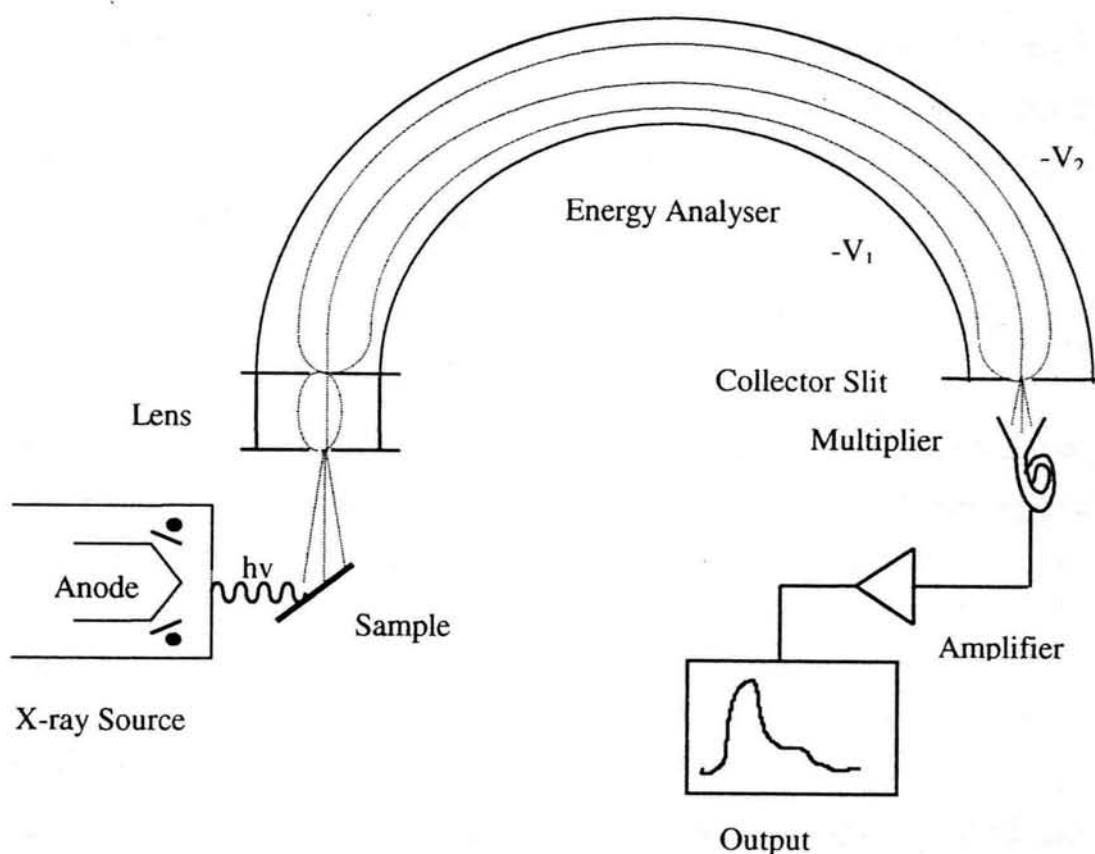
Figure 1.11 Schematic drawing of XPS spectrometer.

accumulated on a PC. The output will plot the binding energies (or kinetic energies) of the photo-ejected electrons against their intensities. Peaks higher in binding energy are indicative of functional groups in which electron density has been withdrawn to greater amounts [42].

1.4.2. Infrared Spectroscopy

A wider picture of the coatings produced during plasma polymerisation can be obtained by probing deeper into the sample surface. Infrared radiation (IR) comprises the electromagnetic radiation between 400 and 4000 cm^{-1} and each chemical functionality present gives rise to characteristic bands in the IR spectrum.

When a certain functionality absorbs electromagnetic radiation of wavelength λ an accompanying increase in energy (ΔE) results which obeys Equation 1.19:

$$\Delta E = \frac{hc}{\lambda}$$

1.19

where h is Planck's constant and c is the speed of light. The absorbance of IR radiation can excite vibrational and rotational energy levels of the molecule. A change in dipole moment must occur in order for the absorption to be allowed. Absorbance can be calculated using the Beer-Lambert equation, Equation 1.20:

$$A = \varepsilon c l$$

1.20

where ε is the permittivity of free space, c is the concentration and l the path length. The absorbance spectrum is obtained by simply plotting the absorbance against wavenumber.

1.4.3. Contact Angle Analysis

Contact angle analysis is a surface sensitive technique which is based on molecular interactions which occur in the top 5 - 10 Å [43]. This information is crucial for many systems involving biocompatibility, lubricity and adhesion, and is often invisible to more expensive and sophisticated microscopic and spectroscopic techniques. There are two types of analysis available, both with advantages and disadvantages. By obtaining contact angles of different liquids possessing different characteristics, surface energy calculations can be made (as explained earlier).

1.4.3.1. Video contact angle (VCA)

This is a sessile drop technique where a known volume of liquid can be dispensed through a motorised micro-syringe onto the surface of interest, Figure 1.12. A CCD camera focused on the droplet resting on the substrate displays the resulting image in real-time on an interfaced PC. A snap-shot of the image can be taken and markers

20

placed around the droplet image. The computer software then calculates the tangent to the droplet shape and computes the contact angle. All substrates that can fit on the sample mount can be used to obtain contact angle data including metals, ceramics, polymers, glass and textiles.
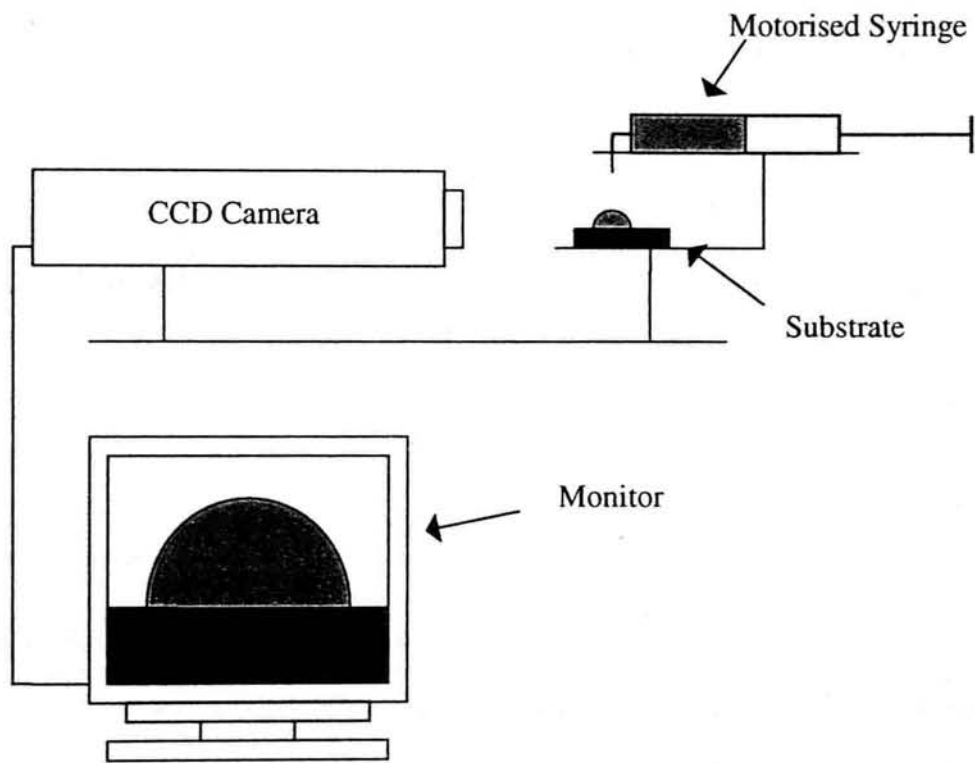

Figure 1.12 Schematic drawing of VCA.

1.4.3.2. Dynamic contact angle (DCA)

This method calculates the contact angle at the three phase solid / liquid / vapour interface, Figure 1.13.
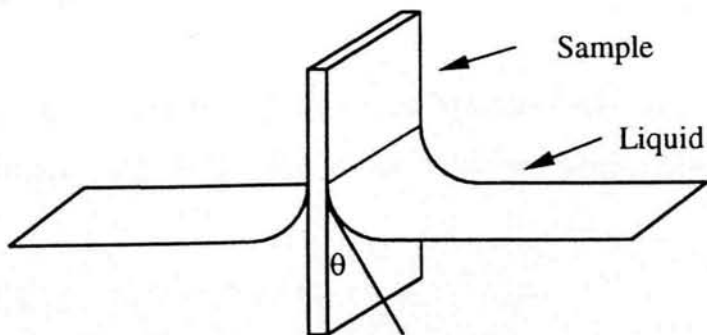
Figure 1.13 Contact angle θ at the solid / liquid / vapour interface.

A solid surface of known perimeter is suspended on a micro-balance, Figure 1.14, where a probe liquid on a motorised stage advances vertically over the surface at a constant rate and produces a unique hysteresis curve.
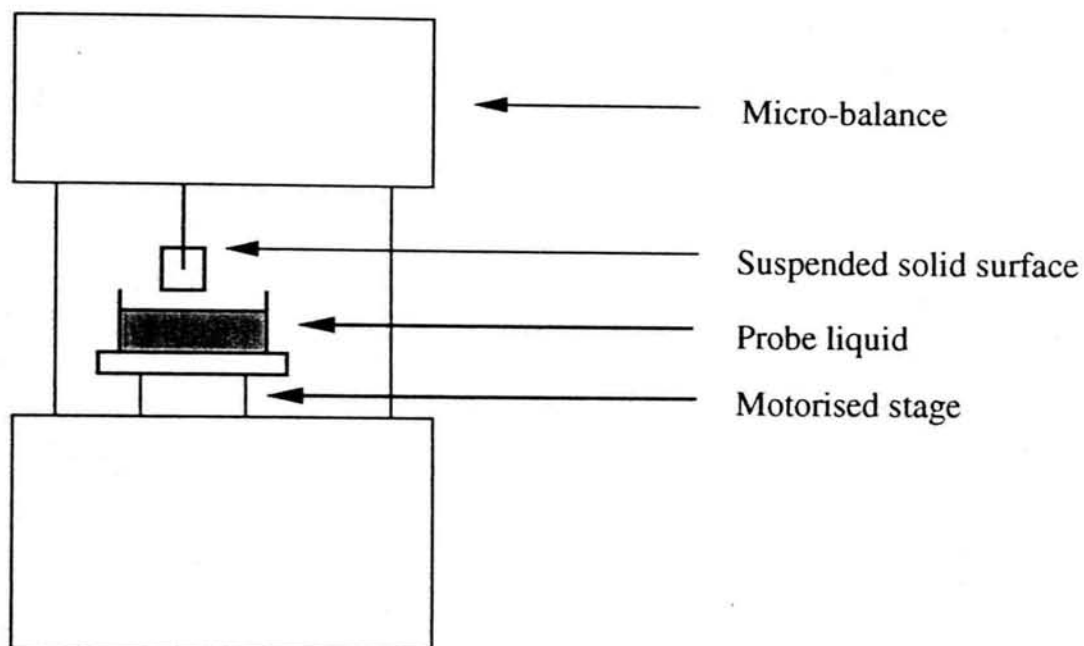
Figure 1.14 Schematic of dynamic contact angle analyser.

As the motorised stage advances towards the sample there is no change in mass experienced on the micro-balance and so the force is constant as the depth increases, Figure 1.15. When the sample plate touches the probe liquid the balance detects a large change in the apparent mass and assigns the immersion depth the zero depth of immersion (ZDOI). A scan of the sample is produced as the probe liquid is advanced and receded over the surface. The advancing and receding contact angles can be determined by extending the advancing and receding plots to the ZDOI line and taking the reading on the force axis.

The dynamic contact angle can be calculated by applying this well established Wilhelmy plate technique [44], [45], [46] to the modified Young equation [47], Equation 1.21:

where F is the wetting force at the meniscus measured by the balance, γ is the surface tension of the probe liquid utilised and p is the perimeter of the meniscus formed at the interface.
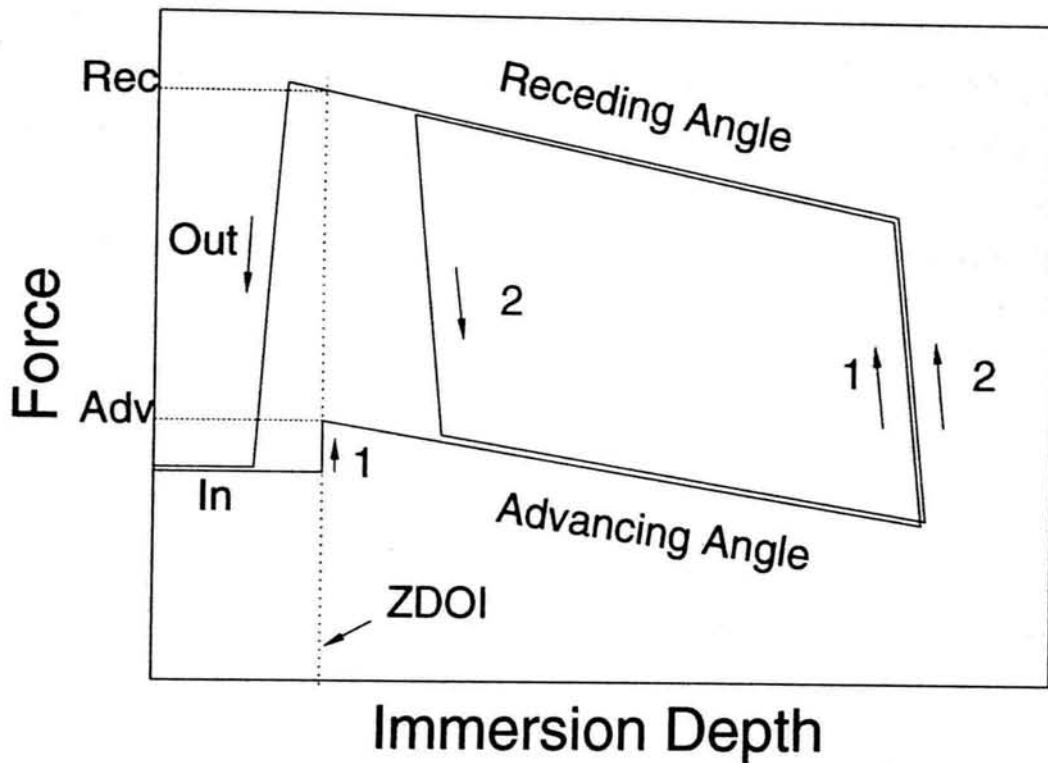
Figure 1.15 Typical surface scan of a two-cycle Wilhelmy plate loop, showing thermodynamic hysteresis.

1.4.4. Deposition Rate Monitor

This is a useful diagnostic tool for studying the mechanisms occurring during plasma polymerisation and how experimental parameters alter the deposition process [48]. It works on the principal that the period of oscillation of a resonating quartz crystal is dependant on its mass and so it is possible to determine the mass of polymer deposited during plasma deposition. The equipment consists of a quartz crystal holder placed in the centre of the plasma chamber connected with water cooling pipes and a coaxial cable to a water supply and deposition rate monitor respectively. The monitor displays a digital reading of the mass in nanograms and by measuring the deposition over a period of time, the deposition rate can be determined.

1.4.5. Atomic Force Microscopy (AFM)

AFM is a technique that maps out the morphology of a sample, by measuring the perturbations of a sharp tip interacting with the surface [49]. The surface is rastered under a tip mounted on an oscillating cantilever utilising a piezoelectric scanner. The oscillation is monitored using a beam-bounce method. The surface is moved so as to keep the interaction between the tip and the sample constant. It is the change in piezo voltage required to maintain a constant force that gives the resulting topographical image [50]. This method is Tapping Mode atomic force microscopy and is ideal for analysis of soft polymer samples, as it eliminates damage caused by contact AFM methods.

1.5. REFERENCES

[1]   I. J. Park, S. B. Lee, C. K. Choi, K. J. Kim, *J. Colloid. Interface. Sci.* **1996**, *181*, 284.

[2]   C. G. DeMarco, A. J. Macquade, S. J. Kennedy, *J. Modern Textile Mag.* **1960**, *2*, 50.

[3]   J. W. Coburn, *IEEE Trans. Plas. Sci.* **1991**, *19*, 6.

[4]   I. Langmuir, *Phys. Rev.* **1929**, *33*, 954.

[5]   J. W. Coburn, *IEEE Trans. Plas. Sci.* **1991**, *19*, 1048.

[6]   A. von Engel in *Electric Plasma: Their Nature and Uses* Taylor & Francis, London, **1983**.

[7]   A. Grill in *Cold Plasma in Materials Technology* IEEE Press, Piscataway, New Jersey, **1994**.

[8]   B. Chapman in *Glow Discharge Processes* John Wiley and Sons, USA, **1980**.

[9]   H. Biederman, Y. Osada, *Adv. Polym. Sci.* **1990**, *95*, 57.

[10]   D. L. Flamm, V. M. Donnelly, D. E. Ibbotson, *J. Vac. Sci. Technol., B* **1983**, *1*, 23.

[11]   F. M. Penning in *Electrical Discharges in Gases* Philips Technical Library, **1957**.

[12]   D. T. Clark, A. Dilks, *J. Polym. Sci., Chem. Ed.* **1977**, *15*, 2321.

[13]   G. S. Oehrlein, *Surf. Sci.* **1997**, *386*, 222.

[14]   C. M. Chan, T. M. Ko, H. Hiraoka, *Surf. Sci. Rep.* **1996**, 24, 3.

[15]   R. K. Wells, J. P. S. Badyal, I. V. V. Drummond, K. S. Robinson, F. J. Street, *J. Chem. Soc. Chem., Commun.* **1991**, *6*, 549.

[16]   S. J. Pearton, F. Ren, *J. Mater. Sci.: Mater. Electronics* **1989**, *5(1)*, 1.

[17]   H. Yasuda, T. Hsu, *J. Polym. Sci., Polym. Chem. Ed.* **1977**, *15*, 81.

[18]   F. Garbassi, M. Morra, E. Occhiello in *Polymer Surfaces: From Physics to Technology* Wiley, Chichester, **1994**.

[19]   A. W. Adamson in *Physical Chemistry of Surfaces* Wiley, 5th Edition, Chichester, **1991**.

[20]   B. W. Cherry in *Polymer Surfaces* Cambridge University, Cambridge, **1981**.

[21] L. H. Sperling in *Introduction to Physical Polymer Science* Wiley, 2nd Edition, Chichester, **1992**.

[22] I. Langmuir in *Collected Works* Pergamon Press, New York, **1960**.

[23] E. Kissa in *Handbook of Fibre Science and Technology* (Eds. M. Lewin, S. B. Sello) Marcel Dekker Inc., Vol 2, Part B, N.Y., **1984**.

[24] B. E. Smart in *Chemistry of Organic Fluorine Compounds* (Eds. M. Hudlicky, A. E. Pavlath) ACS, Washington, **1995**.

[25] R. J. Good in *Contact Angle Wettability and Adhesion* (Ed. K. L. Mittal) VSP, Netherlands, **1993**.

[26] E. N. Dalal, *Langmuir* **1987**, *3*, 1009.

[27] B. W. Cherry in *Aspects of Surface Chemistry and Morphology in Plastics-Surface and Finish* (Eds. S. H. Pinner, W. G. Simpson) Butterworths, London, **1971**.

[28] T. Young, *Philos. Trans. R. Soc. London* **1805**, *95*, 65.

[29] F. M. Fowkes, *Adv. Chem. Ser.* **1964**, *43*, 99.

[30] D. K. Owens, R. C. Wendt, *J. Appl. Polym. Sci.* **1969**, *13*, 1741.

[31] D. H. Kaelble, K. C. Uy, *J. Adhes.* **1970**, 2, 50.

[32] L. A. Girifalco, R. J. Good, *J. Phys. Chem.* **1957**, 61, 904.

[33] F. M. Fowkes, *Ind. Eng. Chem.* **1964**, 56, 40.

[34] S. Wu, *J. Polym. Sci.: Part C* **1971**, *34*, 19.

[35] R. J. Good, N. R. Srivatsa, M. Islam, H. T. L. Huang, C. J. van Oss in *Acid-base Interactions* (Eds. K. L. Mittal H. R. Anderson) VSP, **1991**.

[36] Lord Rayleigh, *Philos. Mag.* **1890**, *30*, 386.

[37] J. D. Andrade, W. Y. Chen, *Surf. Interface. Anal.* **1986**, 9, 418.

[38] M. P. Seah, W. A. Deanch, Surf. Int. Anal. **1979**, *1*, 2.

[39] K. Siegbahn, C. Nordling, A. Fahlman, R. Nordberg, K. Hamrin, J. Hedman, G. Johansson, T. Berkmsrk, S. E. Karlsson, I. Ligren, B. Lindberg in *ESCA, Atomic, Molecular and Solid State Structure Studied by Means of Electron Spectroscopy* Almquist and Wiksells, Uppsala, **1967**.

[40] P. M. A. Sherwood in *Spectroscopy* (Eds. B. P. Straughan, S. Walker) Chapman and Hall, London, **1976**.

[41]   *Practical Surface Analysis* (Eds D. Briggs, M. P. Seah) Wiley, 2nd Edition, Vol. 1, London, **1990**.

[42]   G. Beamson, D. Briggs in *High Resolution XPS of Organic Polymers. The Scienta ESCA300 Database* John Wiley and Sons, Chichester, **1992**.

[43]   J. Domingue, *American Laboratory* **1990**, 22, 50.

[44]   J. D. Andrade, L. M. Smith, in *Surface and Interfacial Aspects of Biomedical Polymers* (Ed. J. D. Andrade) Pleunum, Vol 1, New York, **1985**.

[45]   L. Smith, C. Doyle, D. E. Gregonis, J. D. Andrade, *J. Appl. Polym. Sci.* **1982**, 27, 1269.

[46]   K. G. Tingey, J. D. Andrade, C. W. McGary, Jr, R. J. Zdrahala in *Polymer Surface Dynamics* (Ed. J. D. Andrade) **1983**, 40, 583.

[47]   T. Young, *Philos. Trans*, 95, 65, 82, **1805**.

[48]   J. C. Brice, *Rev. Mod. Phys.* **1985**, 57, 105.

[49]   G. Binnig, C. F. Quate, C. Gerber, *Phys. Rev. Lett.* **1986**, 56, 930.

[50]   *Nanoscope III MultiMode SPM Manual*; Digital Instruments: California, **1992**.

CHAPTER 2

ULTRA LOW SURFACE ENERGY PLASMA POLYMER FILMS

2.1. INTRODUCTION

Water (hydrophobic) and oil (oleophobic) repellency are highly desirable for numerous everyday applications, e.g. aerospace, lithography, sports and outdoor clothing, biomedical layers, protection against environmental fouling, etc. [1], [2], [3], [4]. In the case of flat substrates, it is the chemical nature and packing of functional groups at the surface that have a profound impact on wettability [5], [6]. For instance perfluoroalkyl chains are renowned for their liquid repellency. The tightly bound, non-bonding electron pairs surrounding each fluorine atom core shell in F-C bonds are not easily polarised, and therefore hinder hydrogen bonding and dispersion interactions with polar and non-polar liquids respectively [7]. This type of non-attractive behaviour increases with the degree of fluorine substitution at each carbon centre (i.e. $CF_3 > CF_2 > CF$), and also depends upon perfluoroalkyl chain length (greater withdrawal of

electron density away from the terminal CF_3 group occurs up to a value of $n \approx 7$ for $CF_3(CF_2)_n-$) [8]. It is on this basis, short perfluoroalkyl chains give rise to hydrophobicity, whilst longer perfluorinated chain lengths are necessary for additional oleophobic behaviour. In the latter case, packing efficiently can become sufficient so as to effectively leave just a layer of CF_3 groups exposed at the air-solid interface [9]. Conventional fluoropolymer coating methods for imparting such oil- and water-repellency are typically solvent based [10]. They usually contain combinations of resins, catalysts, homo- and or co-polymers, surfactants, pH adjusters, crosslinking agents, and require heat to effect fixation, etc. [11]. Examples include polymers, copolymers, [12], [13], [14] and crosslinked structures with fluorinated side chains [15]. Surface energy values well below the 18.5 mN m^{-1} for PTFE [16] have been reported for these systems.

An alternative solventless approach is to deposit long liquid repellent perfluoroalkyl chains onto solid surfaces by plasma polymerisation [17]. Such 'cold' plasmas contain heavy particles (gas atoms, molecules, radicals, and ions) at ambient temperature, photons, and 'hot' electrons possessing sufficient kinetic energy to cause bond rupture and further ionisation (thereby sustaining the discharge). The passage of pure organic vapour through this type of medium can lead to the deposition of polymeric films, although structural rearrangement can be a major limitation [18]. Pulsing the electrical discharge on the μs-ms timescale overcomes this drawback by minimising damage to the growing polymer layer, and enabling free radical polymerisation reactions to proceed during the duty cycle off-period [19]. In this study, 1H,1H,2H,2H-heptadecafluorodecyl acrylate ($H_2C=CHCO_2CH_2CH_2(CF_2)_7CF_3$) has been chosen as the feed monomer. This molecule contains a long perfluorinated alkyl chain needed for liquid repellency, and a terminal acrylate group capable of undergoing free radical polymerisation during the pulsed plasma off-period. Only continuous wave plasma polymerisation of fluoroacrylates has been previously investigated [20], [21], [22], [23] and found to yield only limited liquid repellency (typically water and high surface tension alkanes [21]).

2.2. EXPERIMENTAL

Plasma polymerisation experiments were carried out in an inductively coupled cylindrical glow discharge reactor (5 cm diameter, 470 cm^3 volume, base pressure of 3×10^{-2} mbar, and a leak rate of better than 6×10^{-9} moles s^{-1} [24]). This was connected to a two stage Edwards rotary pump via a liquid nitrogen cold trap, a thermocouple pressure gauge, and a monomer tube containing 1H,1H,2H,2H-heptadecafluorodecyl acrylate monomer (Fluorochem, 98% purity, further purified using multiple freeze-thaw cycles). All connections were grease free. An L-C matching unit was used to minimise the standing wave ratio (SWR) of the transmitted power between a 13.56 MHz R.F. generator and the electrical discharge. For pulsed plasma deposition experiments, a signal generator triggered the R.F. source, and an oscilloscope was used to monitor the pulse width and amplitude. The average power <P> delivered to the system was calculated using the following formula [25]:

$$< P >= P_p \left[\frac{t_{on}}{(t_{on} + t_{off})} \right]$$

where $t_{on}/(t_{on} + t_{off})$ is defined as the duty cycle, and P_p is the continuous wave power. A typical experimental run comprised initially scrubbing the reactor with detergent and rinsing with isopropyl alcohol, followed by oven drying. The system was then reassembled and cleaned further with a 50 W air plasma for 30 min. Next, the chamber was vented to air, and the substrate to be coated placed into the centre of the reactor, followed by evacuation back down to base pressure. 1H,1H,2H,2H-heptadecafluorodecyl acrylate vapour was then introduced at a constant pressure of ~0.1 mbar and allowed to purge through the system for 5 min, followed by ignition of the glow discharge. Deposition was terminated after 5 min, and monomer vapour allowed to pass over the substrate for a further 5 min. Subsequently the plasma chamber was evacuated back down to base pressure, and then vented to atmosphere.

Deposition rate measurements were carried out using a gold coated quartz crystal monitor (Inficon XTM/2) located in the centre of the reaction chamber [26]. A control experiment where the monomer vapour was allowed to pass over the substrate for 15 min in the absence of the electrical discharge indicated no deposition.

Bulk phase polymerisation of 1H,1H,2H,2H-heptadecafluorodecyl acrylate comprised placing some uninhibited monomer into a round-bottom flask followed by deoxygenation using a stream of argon. Next, lauroyl peroxide dissolved in toluene solution was added to the monomer, followed by flushing the reaction vessel with argon gas to remove the toluene. The reaction mixture was stirred and warmed to 70°C under a positive flow of argon for 3-4 hours. The solid polymer product was then cooled, dissolved in hexafluoroxylene and precipitated into methanol. Excess solvent was decanted off the gelatinous polymer. Further purification was achieved by agitation in hot methanol followed by decanting. Finally, the polymer was dried in a vacuum oven at 25°C to yield a hard white solid.

A VG ESCALAB MKII electron spectrometer fitted with a non-monochromated Mg Kα X-ray source (1253.6 eV) and a hemispherical analyser operating in the CAE mode (20 eV pass energy) was used for X-ray photoelectron spectroscopy (XPS) analysis of the deposited plasma polymer coatings. The photo-emitted atomic core level electrons were collected at a take-off angle of 30° from the substrate normal, which corresponds to a sampling depth of approximately 1-2 nm for the C(1s) envelope [27]. XPS peaks were fitted using a Marquardt minimisation computer program assuming linear background subtraction. Elemental concentrations were calculated using instrument sensitivity factors determined from chemical standards, C(1s) : O(1s) : F(1s) equals 1.00 : 0.36 : 0.23 respectively. During a typical XPS scan, X-ray beam damage caused less than 1% variation in the F:C ratio, this was sufficiently small that no discernible change was observable in the C(1s) envelope. Complete plasma polymer coverage of the underlying glass substrate was confirmed by the absence of any Si(2p) XPS signal showing through.

A FTIR Mattson Polaris instrument fitted with a Golden Gate single reflection diamond ATR apparatus (Graseby Specac) was used for infrared analysis. Plasma polymerisation depositions were carried out onto sodium chloride plates and analysed using 128 scans at a resolution of 4 cm^{-1}.

A Digital Instruments Nanoscope III atomic force microscope was used to examine the

physical structure of the plasma polymer coatings. The microscope was operated in Tapping Mode, where changes in the oscillation amplitude of the cantilever tip provide a feedback signal for measuring variations in surface topography. All of the AFM images were acquired in air and are presented as unfiltered data. Root-mean-square (RMS) roughness values were obtained from 10 μm x 10 μm images [28].

Sessile drop contact angle measurements were carried out at 20 °C using a video capture apparatus (A.S.T. Products VCA2500XE). The Wilhelmy plate technique (Cahn microbalance, Model DCA322) was employed for dynamic contact angle analysis [29]. In this case, a glass slide coated on both sides was suspended from the microbalance, whilst a motorised stage moved a beaker containing the probe liquid upwards and over the substrate at a speed of 154 μm s^{-1}. The advancing contact angle, θ, corresponds to the tangent at the three phase solid / liquid / vapour interface formed during the initial immersion of the plate, this was calculated by applying the modified Young equation [30]:

$$\cos\theta = \frac{F}{\gamma \times p}$$

where F is the wetting force at the meniscus measured by the microbalance, γ is the surface tension of the probe liquid, and p is the perimeter of the meniscus formed at the three-phase interface. The obtained value of θ was used to calculate the surface energy using two different methods. Firstly, the combined geometric mean-Young's equation was used [30]:

$$(1+\cos\theta)\gamma_i = 2\left[\left(\gamma_i^d \gamma_s^d\right)^{1/2} + \left(\gamma_i^p \gamma_s^p\right)^{1/2}\right]$$

where γ_i is the surface tension of the probe liquid, and γ_i^d and γ_i^p are the respective dispersive and polar (hydrogen bonding and dipolar-dipolar [31]) components [32]. The dispersive (γ_s^d) and polar (γ_s^p) surface energy components for the coating could be calculated by substituting values for water [32] (representative polar liquid, $\gamma_i^d = 22.1$ mN m^{-1} and $\gamma_i^p = 50.7$ mN m^{-1}) and octane [32] (representative non-polar liquid, $\gamma_i^d =$

21.6 mN m^{-1} and $\gamma_l^p = 0.0$ mN m^{-1}) into the equation, and solving the corresponding set of simultaneous equations. Summation of γ_s^d and γ_s^p equates to the total surface energy, γ. An alternative approach is to construct a Zisman plot [6]. This comprises choosing a set of probe liquids from the same homologous series (pentane, hexane, heptane, octane, and dodecane were employed for the plasma polymer surfaces exhibiting no polar contribution [33], [34], [35], [36]) and measuring their advancing contact angles using the Wilhelmy plate apparatus. A plot of the cosine of the advancing contact angle versus the liquid surface tension (γ_l) approximates to a linear relationship called the Zisman plot [6]. By extrapolating the line of best fit to cos $\theta = 1$, the critical surface tension of wetting (referred to from now on as the critical surface tension) for the solid surface, γ_c, is obtained. Any liquid with a surface tension smaller than this value forms a zero contact angle with the coating. The Wilhelmy plate apparatus was also used to check that the surface tension of each probe liquid was consistent with reported literature values [32], Table 2.1.

Repellency	Liquid	Surface Tension [32] / mN m^{-1} (at 20 °C)
Hydrophobicity	Water	72.8
	Isopropyl alcohol	21.3
Oleophobicity	Hexadecane	27.5
	Tetradecane	26.6
	Dodecane	25.4
	Decane	23.8
	Octane	21.6
	Heptane	20.1
	Hexane	18.4
	Pentane	16.1

Table 2.1 Surface tensions of probe liquids.

2.3. RESULTS

The C(1s) XPS spectra of the deposited plasma polymer layers could be fitted to 7 Gaussian Mg $K\alpha_{1,2}$ components each with 3 variables, height, centre and width, resulting in 21 variables of which 12 are fixed. The peaks have equal full-width-at-half-maximum (FWHM) as these are independent of the kinetic energy of the peak position [27], [37], [38]: $\underline{C}_xH_y$ at 285.0 eV, $\underline{C}$-C(O)=O at 285.7 eV, $\underline{C}$-O/$\underline{C}$-CF$_n$ at 286.6 eV, $\underline{C}$F at 287.8 eV, O-$\underline{C}$=O/$\underline{C}$F-CF$_n$ at 289.0 eV, $\underline{C}$F$_2$ at 291.2 eV, and $\underline{C}$F$_3$ at 293.3 eV (corresponding Mg $K\alpha_{3,4}$ satellite peaks were shifted by ~9 eV towards lower binding energy [27]), Figure 2.1. The fitting involved initially placing one peak at the steepest side of the envelope and applying a correction factor to adjust the centre to literature values. A temporary width of around 2.3 eV was assumed. The additional peaks were added at known positions with equal width. Computer optimisation of the heights, and the width of the initial peak, were carried out until the line of best fit passed through the data points. At each stage all peak widths were corrected to that of the initial.

The oxygenated / hydrogenated carbon centres originate from the acrylate group in the monomer. In the case of continuous wave (CW) plasma polymerisation experiments, the whole range of functionalities were found to be present in significant amounts, Figure 2.1 and Table 2.2.

Conditions	F:C Ratio	%$\underline{C}$F$_2$	%$\underline{C}$F$_3$
Theoretical	1.31	53.8	7.7
Conventional polymer	1.22 ± 0.02	44.8 ± 0.1	14.1 ± 0.6
Optimum pulsed plasma	1.33 ± 0.06	46.7 ± 0.5	14.6 ± 1.3
5 W CW plasma	0.50 ± 0.18	17.2 ± 4.9	3.9 ± 1.4

Table 2.2 Compilation of the theoretical (corresponding to the monomer structure, $CH_2=CHCO_2CH_2CH_2C_8F_{17}$) and actual chemical environments measured by XPS.
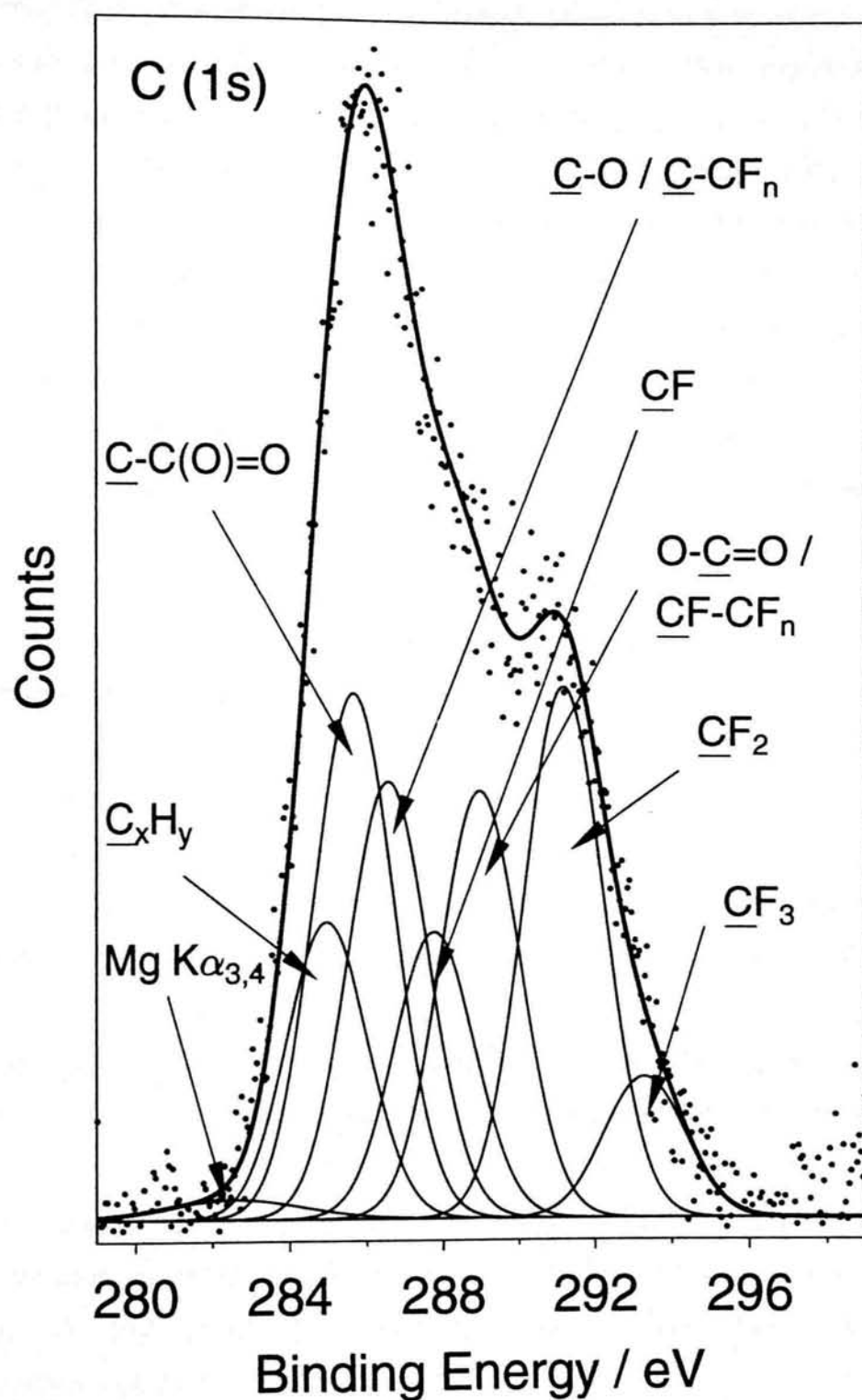
Figure 2.1 C(1s) XPS spectrum of 5 W continuous wave plasma polymerised 1H,1H,2H,2H-heptadecafluorodecyl acrylate deposited onto a flat glass substrate.

Decreasing the duty cycle during pulsed plasma polymerisation improved $>\underline{C}F_2$ group incorporation, eventually becoming close to the theoretically expected value for complete structural retention of the perfluoroalkyl chain, Figures 2.2a, 2.2b and 2.3 and Table 2.2. Under these conditions, the concentration of CF_3 functionalities present in the C(1s) envelope appears to be greater than predicted by the monomer structure, Table 2.2. This is most likely due to the surface sensitivity of the XPS technique, yielding a more intense signal from the terminal CF_3 group, aligned at the solid-air interface. The C(1s) signal from the ester linkages is consistent with the XPS sampling depth [27] (approximately 1-2 nm) being greater than the length of the perfluoroalkyl side-chain [39]. Comparable spectra were obtained for the conventional polymer prepared by bulk polymerisation of the monomer, Table 2.2.

Corresponding differences between continuous wave and pulsed plasma deposition were also evident in the infrared spectra, Figure 2.4 and Table 2.3. The sharpness of the spectral features associated with the liquid monomer were retained for the pulsed plasma polymer coatings; whereas spectral broadening was evident for continuous wave conditions as a consequence of the higher powers leading to extensive fragmentation, rearrangement, and cross-linking reactions of the parent molecule. Disappearance of the characteristic acrylate carbon-carbon double bond absorption bands at 1640 cm^{-1}, 1625 cm^{-1}, 1412 cm^{-1}, 1298 cm^{-1}, 986 cm^{-1}, 970 cm^{-1}, and 812 cm^{-1} during pulsed plasma polymerisation is consistent with the reaction proceeding via the acrylate double bond, whilst leaving the associated ester carbonyl group at 1734-1736 cm^{-1} intact.

The deposition rate was found to pass through a maximum with decreasing average power during pulsed plasma polymerisation, Figures 2.5a and 2.5b. Within this general trend, the observed spread of values for a specific average power suggests some dependency on the duty cycle parameters.

AFM studies gave a RMS roughness value of 0.7 nm for the glass substrate and approximately 7 nm for the continuous wave and pulsed plasma polymer films (although their respective morphologies were different), Figures 2.6a, 2.6b and 2.6c. This compares with RMS roughness values of 0.5 nm reported for conventional solution phase polymerised perfluoroacrylates [40].
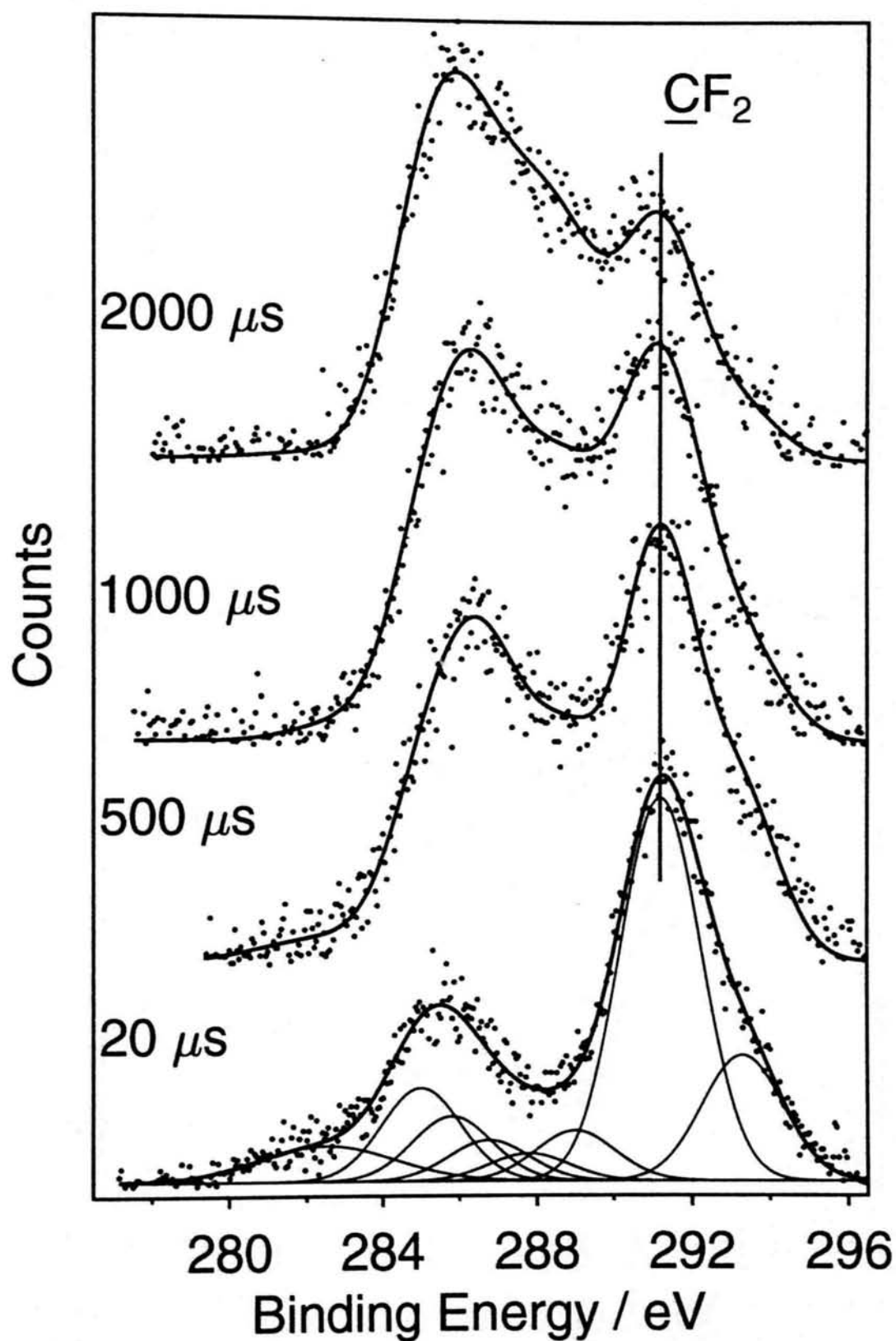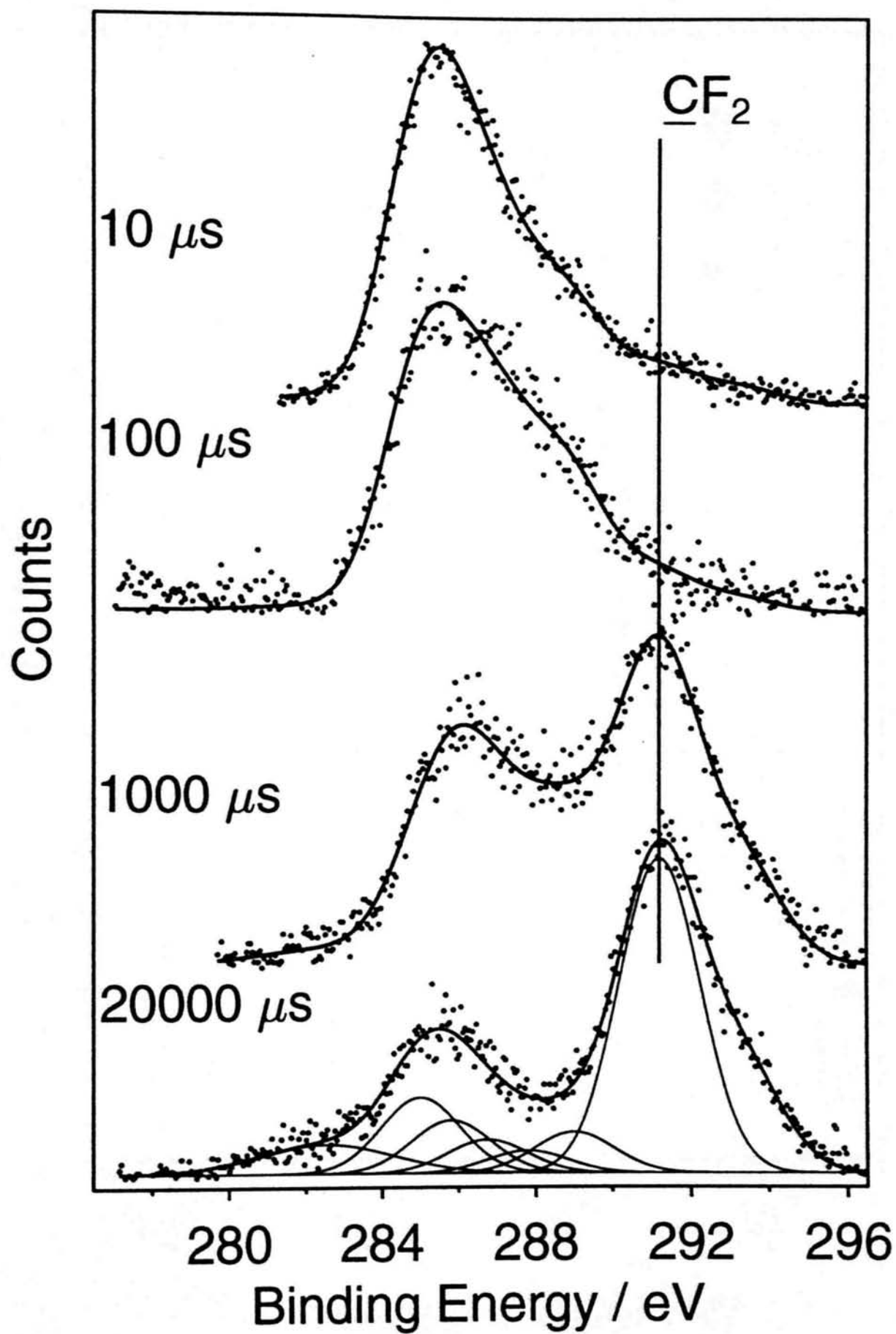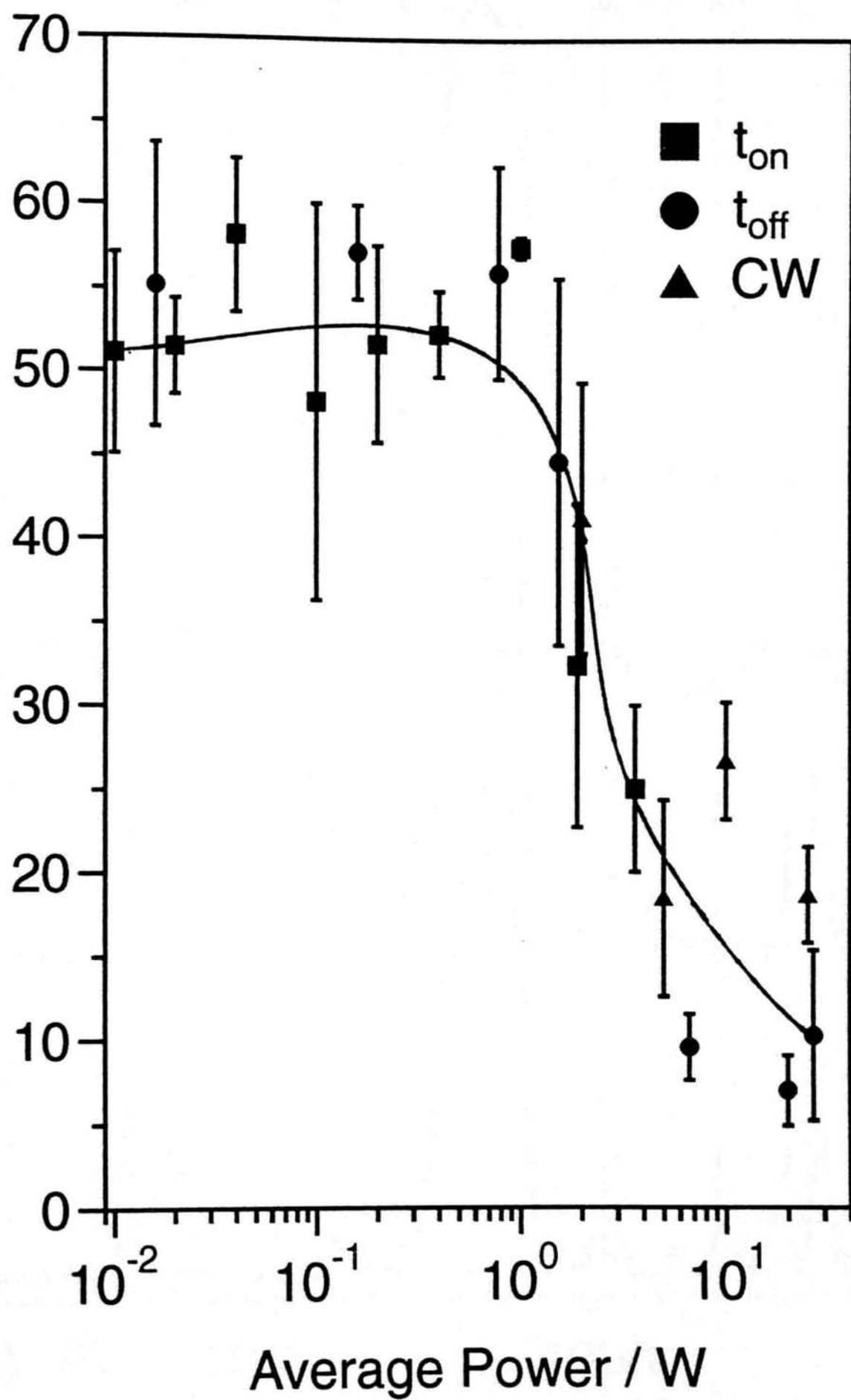
Figure 2.2a C(1s) XPS spectra of pulsed plasma polymerisation of 1H,1H,2H,2H-heptadecafluorodecyl acrylate with varying t_{on} (t_{off} = 20,000 μs, P_p = 40 W).
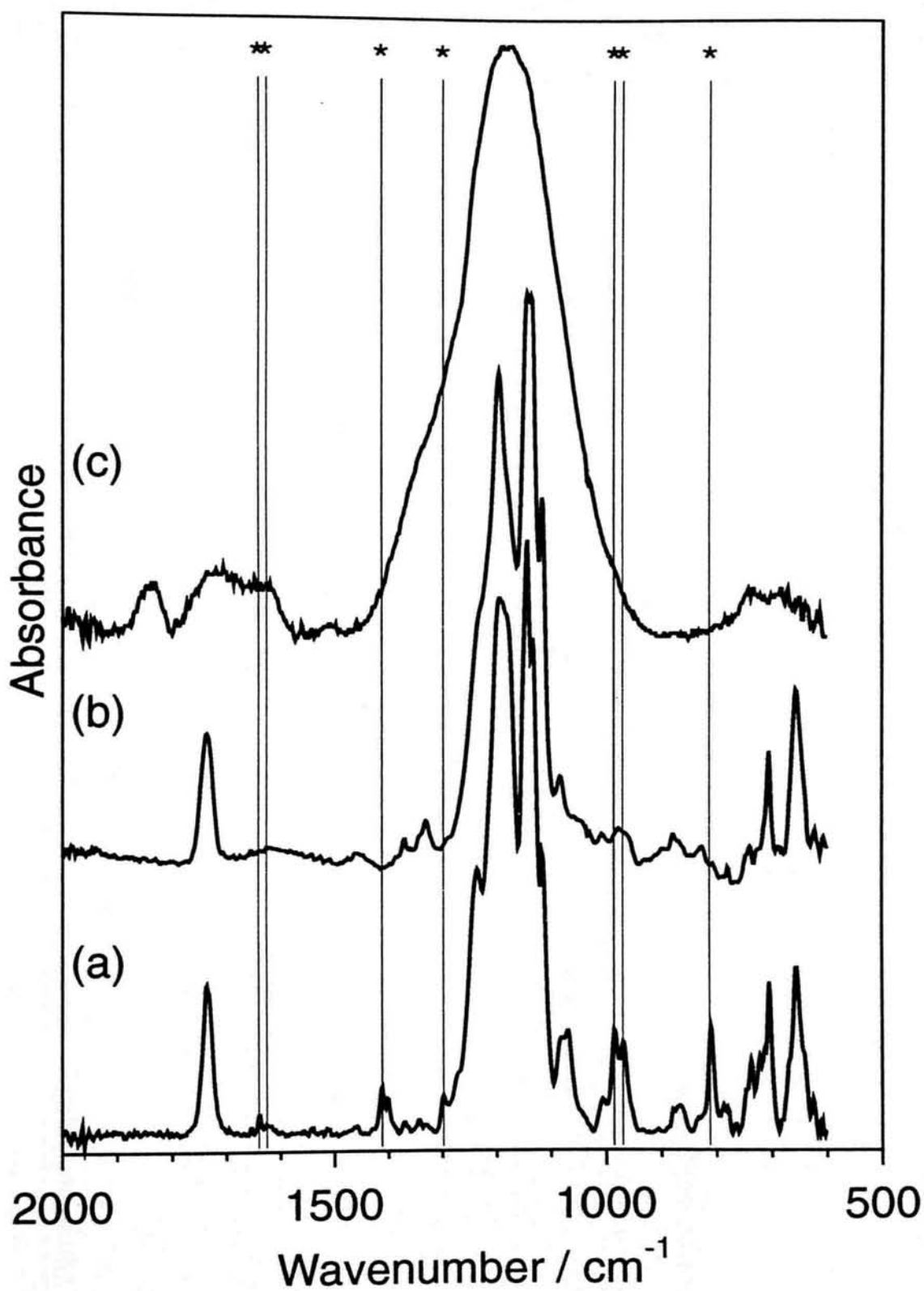
Figure 2.4 Comparison of infrared spectra: (a) 1H,1H,2H,2H-heptadecafluorodecyl acrylate monomer; (b) pulsed plasma polymerisation (t_{on} = 20 μs, t_{off} = 20,000 μs, P_p = 40 W); and (c) 5 W continuous wave plasma polymerisation. NB * denotes acrylate carbon-carbon double bond absorption band.